LAWRENCE
LIVERMORE
NATIONAL
LABORATORY

UCRL-TR-214631

Deducing the 237U(n,f) cross-section using the Surrogate Ratio Method

J. T. Burke, L. A. Bernstein, J. Escher, L. Ahle, J. A. Church, F. Dietrich, K. J. Moody, E. B. Norman, L. W. Phair, P. Fallon, R. Clark, M. Delaplanque, M. Descovich, M. Cromaz, I. Y. Lee, A. O. Macchiavelli, M. A. McMahan, L. G. Moretto, E. Rodriguez-Vieitez, F. S. Stephens

August 16, 2005

This work was performed under the auspices of the U.S. Department of Energy by University of California, Lawrence Livermore National Laboratory under Contract W-7405-Eng-48.

Deducing the ^{237}U(n,f) cross-section using the Surrogate Ratio Method

J.T. Burke,* L.A. Bernstein, J. Escher, L. Ahle, J.A. Church, F.S. Dietrich, K.J. Moody, and E.B. Norman

Lawrence Livermore National Laboratory, Livermore, California, 94550

L.W. Phair, P. Fallon, R.M. Clark, M.A. Delaplanque, M. Descovich, M. Cromaz, I.Y. Lee, A.O. Macchiavelli, M.A. McMahan, L.G. Moretto, E. Rodriguez–Vieitez, and F.S. Stephens

Lawrence Berkeley National Laboratory, Berkeley, California, 94720

(Dated: September 12, 2005)

Abstract

We have deduced the ^{237}U(n,f) cross-section over an equivalent neutron energy range of 0 to 20 MeV using the Surrogate Ratio method. A 55 MeV $^{4}He^{2+}$ beam from the 88 Inch Cyclotron at Lawrence Berkeley National Laboratory was used to induce fission in the following reactions $^{238}U(\alpha,\alpha' f)$ and $^{236}U(\alpha,\alpha' f)$. The ^{238}U reaction was a surrogate for $^{237}U(n,f)$ and the ^{236}U reaction was used as a surrogate for $^{235}U(n,f)$. The energies of the scattered alpha particles were detected in a fully depleted segmented silicon telescope array (STARS) over an angle range of 35^o to 60^o with respect to the beam axis. The fission fragments were detected in a third independent silicon detector located at backward angles between 106^o to 131^o.

*Electronic address: burke26@llnl.gov

I. INTRODUCTION

Neutron-induced fission cross sections are of interest for a variety of applied and basic science reasons. To further our understanding of fission we have explored a "Surrogate Ratio method" which allows us to determine fission cross sections of short lived (T<1 year) nuclei. The Surrogate Ratio method requires a nearby nucleus to have a well-measured fission cross section. This technique removes and/or reduces a large number of systematic and theoretical uncertainties related to the direct Surrogate Method [2, 3].

We have deduced the ^{237}U(n,f) cross section over an equivalent neutron energy range from 0 to 20 MeV. The uranium isotopes ^{238}U and ^{236}U were excited to energies of 31 MeV via inelastic scattering by 55 MeV alpha particles, and the resulting fission fragments were measured in coincidence with the outgoing alphas. ^{238}U was used as a surrogate for ^{237}U and ^{236}U was a surrogate for ^{235}U. These measurements allowed us to infer the ratio of the ^{237}U(n,f) to ^{235}U(n,f) cross sections. Since the ^{235}U(n,f) cross section is well known, we were able to deduce the ^{237}U(n,f) cross section. We use the same approach that was employed by Plettner et al. [1]. In this report, we review the Surrogate Ratio method as it pertains to fission. In sections III through VII we describe the experimental apparatus, detector calibration, data and analysis, systematic uncertainties, and finally the resulting ^{237}U(n,f) deduced cross section. For completeness tables of the data and results can be found in appendix A and B.

II. THE SURROGATE RATIO METHOD

The "Surrogate Ratio method" or, simply, the "Ratio method" is an indirect technique that allows one to determine cross sections for compound-nucleus reactions involving difficult to produce targets. The method employs an approximate version of the so-called "Surrogate nuclear reaction approach" to relate reactions on a pair of targets and to infer the cross section on one of these if the other is known. In this report we use the known ^{235}U(n, f) cross section to obtain the cross section for ^{237}U(n, f) for neutron energies up to 20 MeV. The following reviews the Surrogate nuclear reaction idea, explains the motivation for considering simplifications of the approach, and outlines the Ratio method.

The Surrogate nuclear reaction technique is an indirect method for determining the cross

section for a particular type of "desired" reaction, namely a two-step reaction, $a + A \rightarrow B^* \rightarrow c + C$, that proceeds through a compound nuclear state B^*, a highly excited state in statistical equilibrium [4–13]. The formation and decay of a compound nucleus (CN) are, by definition, independent of each other (for each angular momentum and parity value). In such situations, the cross section for the "desired" reaction can be (somewhat schematically) expressed as

$$\sigma_{\alpha\chi}(E_a) \; = \; \sum_{J,\pi} \sigma_\alpha^{CN}(E_{ex}, J, \pi) \;\; G_\chi^{CN}(E_{ex}, J, \pi) \; . \tag{1}$$

Here α denotes the entrance channel $a + A$ and χ represents the relevant exit channel $c + C$. E_a is the kinetic energy of the projectile a and E_{ex} is the excitation energy of the compound nucleus B^*; they are related via the separation energy S_a of the projectile in the nucleus B: $E_{ex} = S_a + E_a$. In this present work, we are interested in the reactions $n+^{235}\mathrm{U} \rightarrow {}^{236}\mathrm{U}^* \rightarrow$ *fission* and $n+^{237}\mathrm{U} \rightarrow {}^{238}\mathrm{U}^* \rightarrow$ *fission*. In many cases the formation cross section $\sigma_\alpha^{CN} = \sigma(a + A \rightarrow B^*)$ can be calculated adequately by using optical potentials, while the theoretical decay probabilities G_χ^{CN} for the different channels χ are often quite uncertain. The objective of the Surrogate method is to determine or constrain these decay probabilities experimentally.

In a Surrogate experiment, the compound nucleus B^* is produced via an alternative ("Surrogate"), direct reaction $d + D \rightarrow b + B^*$ and the decay of B^* is observed in coincidence with the outgoing particle b. In this experiment, the relevant compound nuclei ${}^{236}\mathrm{U}^*$ and ${}^{238}\mathrm{U}^*$ were produced via inelastic alpha scattering, $\alpha+{}^{x}\mathrm{U} \rightarrow \alpha'+{}^{x}\mathrm{U}^*$, with $x = 236$ and 238 respectively. Fission fragments were detected in coincidence with scattered alpha particles. The probability for forming B^* in the Surrogate reaction (with specific values for the excitation energy E_{ex}, angular momentum J, and parity π) is $F_\delta^{CN}(E_{ex}, J, \pi)$, where δ refers to the entrance channel $d+D$. The quantity

$$P_{\delta\chi}(E_{ex}) = \sum_{J,\pi} F_\delta^{CN}(E_{ex}, J, \pi) \;\; G_\chi^{CN}(E_{ex}, J, \pi) \; , \tag{2}$$

which gives the probability that the compound nucleus B^* was formed with energy E_{ex} and decayed into channel χ, can in principle be obtained experimentally.

The direct-reaction probabilities $F_\delta^{CN}(E_{ex}, J, \pi)$ have to be determined theoretically, so that the branching ratios $G_\chi^{CN}(E_{ex}, J, \pi)$ can be extracted from the measurements. In practice, the decay of the compound nucleus is modeled using statistical reaction theory and the

$G_\chi^{CN}(E_{ex}, J, \pi)$ are obtained by adjusting parameters in the calculations to reproduce the measured decay probabilities $P_{\delta\chi}(E_{ex})$. Subsequently, the branching ratios obtained in this manner are inserted in Eq. 1 to yield the desired reaction cross section.

The experimental determination of the decay probability $P_{\delta\chi}(E_{ex}) = N_{\delta\chi}/N_\delta$ requires that both the number of b-χ coincidences ($N_{\delta\chi}$) and the number of reaction events (N_δ) (the total number of inelastically scattered alpha particles in the present case) are accurately determined. If target contaminants are present, it becomes very difficult, if not impossible to determine a reliable value for N_δ.

The "Surrogate Ratio method" eliminates the need to accurately measure N_δ, the total number of reaction events, which has been the source of the largest uncertainty in Surrogate experiments performed recently [1, 2]. Under the proper circumstances it also reduces or removes dependence on the angular distribution of fission fragments, which is not well characterized in the present experiments. The goal of the Ratio method is to experimentally determine the ratio

$$R(E) \;=\; \frac{\sigma_{\alpha_1\chi_1}(E)}{\sigma_{\alpha_2\chi_2}(E)} \tag{3}$$

of the cross sections of two compound-nucleus reactions, $a_1 + A_1 \rightarrow B_1^* \rightarrow c_1 + C_1$ and $a_2 + A_2 \rightarrow B_2^* \rightarrow c_2 + C_2$, for the same excitation energy, $E \equiv E_{ex_1} = E_{ex_2}$ of both compound nuclei. An independent determination of one of the above cross sections then allows one to infer the other by using the ratio $R(E)$.

Under certain conditions [14, 15] the branching ratios $G_\chi^{CN}(E_{ex}, J, \pi)$ become independent of J and π, i.e. the Weisskopf-Ewing limit of the statistical Hauser-Feshbach theory applies. The form of the cross section (for the desired reaction) simplifies to $\sigma_{\alpha\chi}^{WE}(E_{ex}) = \sigma_\alpha^{CN}(E_{ex})\ \mathcal{G}_\chi^{CN}(E_{ex})$ where $\sigma_\alpha^{CN}(E_{ex}) = \sum_{J\Pi} \sigma_\alpha^{CN}(E_{ex}, J, \pi)$ is the reaction cross section describing the formation of the compound nucleus at energy E_{ex} and $\mathcal{G}_\chi^{CN}(E_{ex})$ denotes the $J\pi$-independent branching ratio for the exit channel χ. In the Weisskopf-Ewing limit, the ratio $R(E_{ex})$ can be written as:

$$R(E_{ex}) \;=\; \frac{\sigma_{\alpha_1}^{CN}(E_{ex})\ \mathcal{G}_{\chi_1}^{CN}(E_{ex})}{\sigma_{\alpha_2}^{CN}(E_{ex})\ \mathcal{G}_{\chi_2}^{CN}(E_{ex})}\,, \tag{4}$$

with branching ratios $\mathcal{G}_\chi^{CN}$ that are independent of the $J\pi$ population of the compound nuclei under consideration. For most cases of interest the compound-nucleus formation cross sections $\sigma_{\alpha_1}^{CN}$ and $\sigma_{\alpha_2}^{CN}$ can be calculated using an optical model. To determine $\mathcal{G}_{\chi_1}^{CN}/\mathcal{G}_{\chi_2}^{CN}$, two

experiments are carried out. Both use the same direct-reaction mechanism $D(d,b)B^*$, but different targets D_1 and D_2 to create the relevant compound nuclei B_1^* and B_2^* respectively. For each experiment, the number of coincidence events, $N^{(1)}_{\delta_1\chi_1}$ and $N^{(2)}_{\delta_2\chi_2}$, are measured.

In the present case, ^{236}U(α,α')^{236}U* and ^{238}U(α,α')^{238}U* experiments were carried out and α-*fission* coincidences were measured. The same experimental setup was employed for both cases. The ratio of the branching ratios into the desired channel for the compound nuclei created in the two reactions is given by

$$\frac{\mathcal{G}^{CN}_{\chi_1}(E_{ex})}{\mathcal{G}^{CN}_{\chi_2}(E_{ex})} \;=\; \frac{N^{(1)}_{\delta_1\chi_1}(E_{ex})}{N^{(2)}_{\delta_2\chi_2}(E_{ex})} \times \frac{N^{(2)}_{\delta_2}(E_{ex})}{N^{(1)}_{\delta_1}(E_{ex})} \; . \tag{5}$$

If both experiments give the same number of reaction events, $N^{(1)}_{\delta_1} \approx N^{(2)}_{\delta_2}$, the ratio of the decay probabilities simply equals the ratio of the coincidence events and the quantity $R(E_{ex})$ becomes:

$$R(E_{ex}) \;=\; \frac{\sigma^{CN}_{\alpha_1}(E_{ex})\; N^{(1)}_{\delta_1\chi_1}(E_{ex})}{\sigma^{CN}_{\alpha_2}(E_{ex})\; N^{(2)}_{\delta_2\chi_2}(E_{ex})} \; . \tag{6}$$

In practice it is unlikely that both experiments yield the same number of reaction events and it becomes necessary to apply a correction to account for the difference in target thickness, integrated beam on target, and live time of the data acquisition for the two experiments.

III. EXPERIMENTAL APPARATUS

The experiment was performed at the 88 Inch Cyclotron at Lawrence Berkeley National Laboratory using the Silicon Telescope Array for Reactions Studies (STARS). Inelastic scattering of alpha particles in the reactions $^{238}U(\alpha,\alpha' f)$ and $^{236}U(\alpha,\alpha' f)$ were measured using the STARS scattering chamber shown in figure 1. The silicon telescope produces differential energy loss in the thin (ΔE) and thick (E) detectors which enables particle identification. The ΔE detector was a Micron S2 140 μm thick silicon detector. The E detector was a Micron S2 1000 μm thick detector. Each S2 detector has 48 rings on one side and 16 sectors on the other. For this experiment both detectors had pairs of adjacent rings and sectors bussed together to form twenty-four 1 mm wide rings and 8 sectors from the original 16. The targets were located 16 mm upstream from the front face of the ΔE detector. The ΔE

and E detectors were spaced 3 mm apart. The beam spot on the target was approximately 3 mm in diameter. This geometry leads to an angular detection range in θ (the angle formed between the beam axis and the scattered alpha particle) from 35^o to 60^o. The trajectory of an alpha particle was determined by which rings in the ΔE and E detector were triggered. The angular resolution limited the precision of the recoil energy correction applied in section V. The fission fragments were detected in a third 140 μm Micron S2 detector located 10 mm upstream of the target. The adjacent rings and sectors of this detector were also bussed together. The fission detector covered an angle range of 106^o to 131^o with respect to the beam axis. A 4.44 $\frac{mg}{cm^2}$ aluminum foil was placed between the target and the silicon telescope. The aluminum foil served a dual purpose. The foil ranged out the fission fragments thereby protecting the ΔE detector from damage which would reduce its energy resolution. The foil was also biased to 300 V during the experiment to help reduce the presence of delta electrons produced in the target. Without bias voltage applied to the aluminum foil the leakage current in the silicon detectors changed rapidly while beam was on target. The changing leakage current could then affect the gain of the ΔE and E detectors of the telescope.

The ΔE, E, and fission detectors were biased with 30 V, 105 V, and 30 V respectively. The signals from the rings and sectors of the ΔE and E detector were conducted through the vacuum chamber wall by four straight through 34 pin connectors potted into a custom made NEMA-G10 vacuum flange. The signals were pre-amplified by 64 individual 45 mV/MeV pre-amplifiers located on the side of the STARS scattering chamber. The amplified signals were connected to four 16 channel CAEN N568B shapers by 64 individual 10 m long RG-174 cables. Similarily, the signals from the rings and sectors of the fission detector were pre-amplified by sixteen individual 8 mV/MeV pre-amplifiers located on the other side of the STARS scattering chamber.

The fast output of the CAEN N568B shapers were connected to LeCroy 1806 discriminators modified to be leading edge. The discriminator thresholds were set at 60 mV which corresponds to an energy threshold of approximately 800 keV per channel. At least one hit in the ΔE and E detectors were required to form the particle trigger. Once a valid trigger occured, the delayed shaped slow output of the shaper channels were digitized by 96 channels of SILENA analog to digital converters (ADCs). The gate to the SILENA ADCs was approximately 7 μs long.

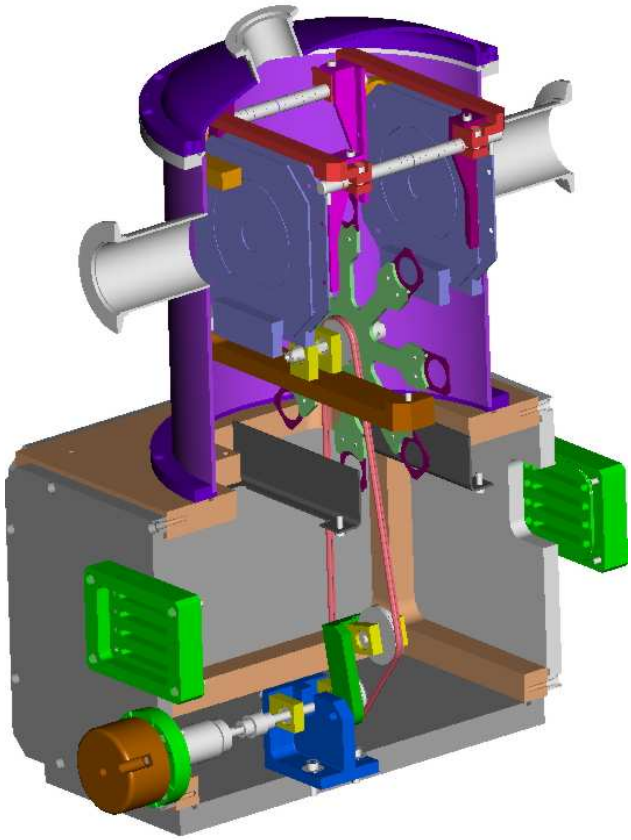

FIG. 1: Cut away view of the STARS scattering chamber. The eight position target wheel is visible in the center of the chamber. Silicon telescopes are shown on either side of the target wheel. In this experiment, one silicon telescope was located down stream for particle identification while only one silicon detector was located upstream serving as the fission detector.

IV. DETECTOR CALIBRATION

The ΔE and E silicon detectors were calibrated using a ^{226}Ra alpha source. The five strong emitted alpha energies from the decay chain are 7686.8 keV, 6002.4 keV, 5489.5 keV, 5304.4 keV, and 4784.3 keV. A calibration was performed by placing the ^{226}Ra source approximately 15 mm from the front face of a detector. Data were acquired with a singles trigger until sufficient statistics were obtained. A typical calibration spectrum is shown in figure 2. The peaks were fit with a skewed gaussian. The skewed gaussian accounts for the effects of incomplete charge collection in the silicon. Typical values for σ were between

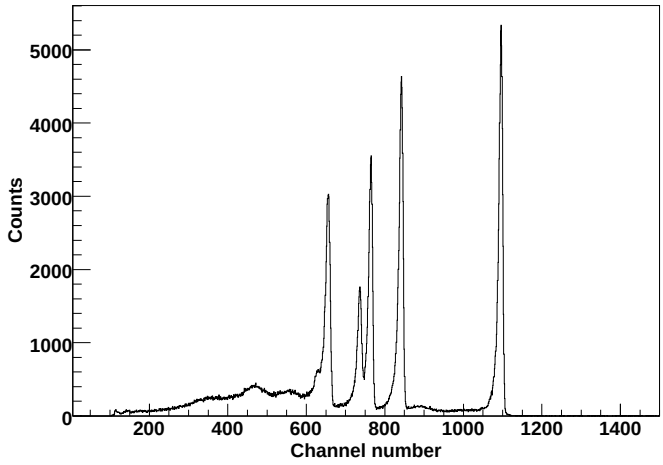

FIG. 2: A typical ^{226}Ra calibration spectrum for an individual ring. The data show the five dominant alpha particles present in the ^{226}Ra decay chain versus channel number in the SILENA ADC.

31 to 46 keV for the rings on the ΔE detector and 22 to 30 keV for the rings on the E detector. The sectors of both detectors had a factor of approximately 1.4 poorer energy resolution (ΔE/E). In order to obtain the best energy resolution possible the rings were used to reconstruct the energy of the alpha particle events. The one σ energy resolution of the combined detectors was taken as the sum of the squares of the individual uncertainties and ranged between 38 keV to 55 keV.

V. DATA AND ANALYSIS

Data were taken over a period of five consecutive days at the 88 Inch Cyclotron. The 88 Inch Cyclotron generated a 55 MeV beam of alpha particles with an intensity between 2 to 5 pnA. The ΔE-E overlap coincidence time window was adjusted to be approximately 50 ns. The ^{238}U fission data were obtained from a self supporting metallic 3619 ± 72 angstrom (585 ± 23 $\frac{\mu g}{cm^2}$) thick ^{238}U foil. The ^{236}U fission data were obtained using a uranyl nitrate $^{236}UO_2(NO_3)_2$ target consisting of 99.68% ^{236}U and 0.32% ^{234}U electroplated onto a 2.3 $\frac{mg}{cm^2}$ Ta foil. The ^{236}U foil had an areal density of approximately 184 ± 9 $\frac{\mu g}{cm^2}$. The areal density of each target was determined by its area and specific activity. The master trigger rate

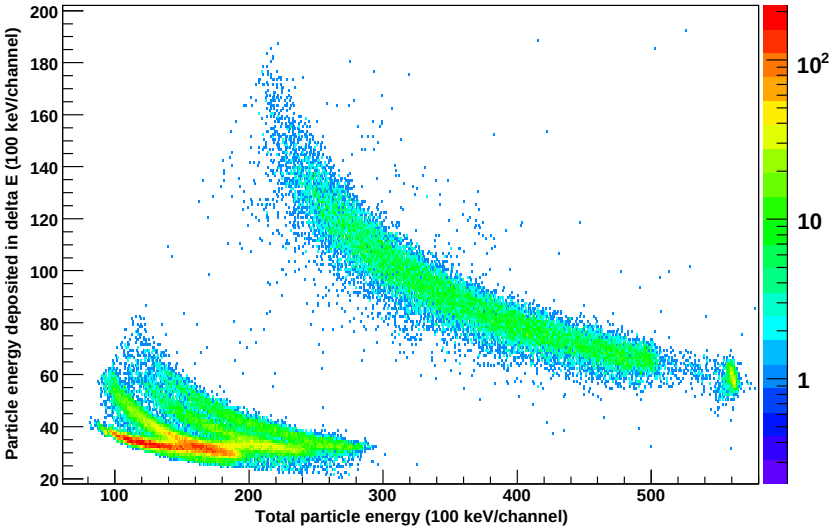

FIG. 3: Delta E versus E plot obtained from nominally 55 MeV alpha particle incident on ^{238}U in coincidence with fission events. Starting in the lower left corner we see protons, deuterons, and tritons. The large band in the middle of the plot represents alpha particles.

for coincident events ranged between 4 kHz to 6 kHz during the experiment. The system deadtime was fixed by a master gate width of 70 μs. At the master trigger rates of 4 kHz and 6 kHz the system deadtime was 28 % and 42 % respectively. The fission detector singles rate was considerably higher at 40 kHz. This was due to a large (approximately 1 barn) ^{238}U(α, f) fusion fission cross section.

The protons, deuterons, tritons, ^{3}He and alpha particles were uniquely identified by plotting the ΔE energy versus the total energy (ΔE + E) to create a particle idenitification plot (PID) plot as shown in figure 3. The PID plot for each ring was linearized to create an effective thickness versus energy plot. The effective thickness energy plot was generated using the following linearization function where R is the range, E_{tot} is the total particle energy, and E is the energy deposited in the E detector.

$$R = 15.0 \times (E_{tot}^{1.75} - E^{1.75}) \tag{7}$$

Figure 4 shows a typical effective thickness energy curve for an individual ring. Alpha particle events were defined as particles that occured within an energy range of 2 sigma (approximately 400 keV) of the alpha particle band. The alpha particle discrimination is evident in figure 5. Events in the fission detector greater than 6 MeV were identified as fission

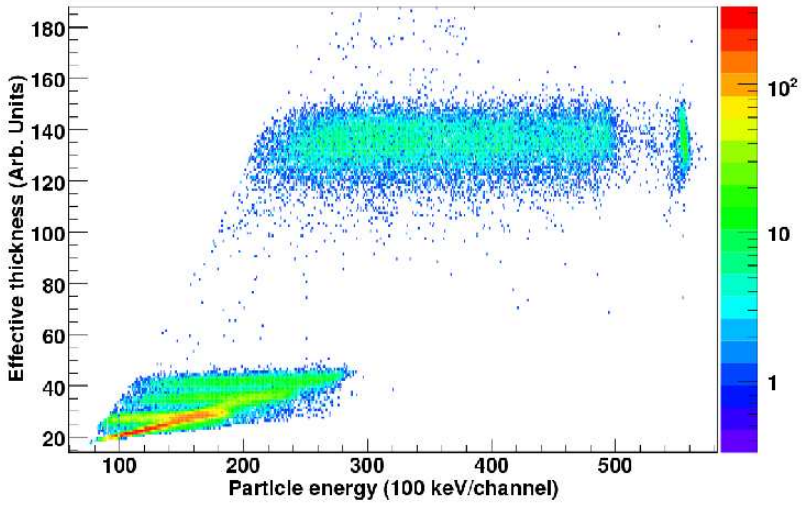

FIG. 4: Effective thickness energy curve. Alpha particles can be seen in the top band. The three bands in the lower left hand corner starting from the bottom are protons, deuterons, and tritons respectively.

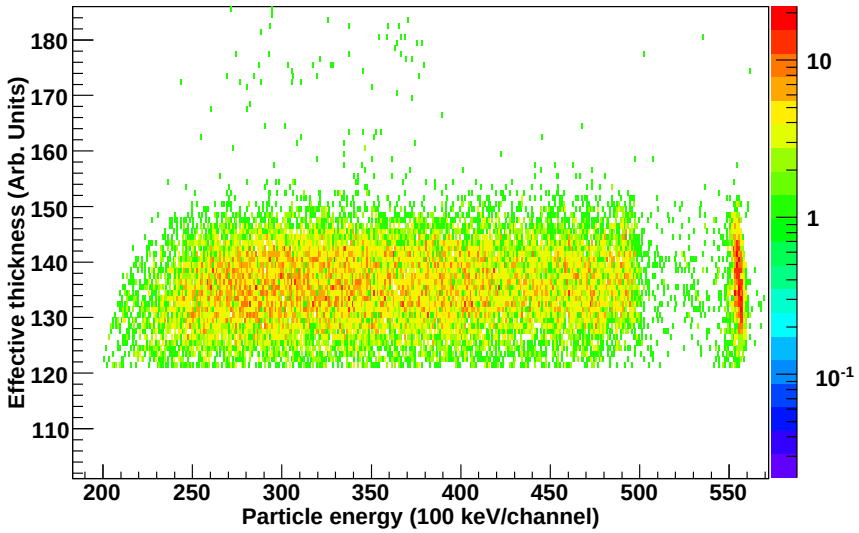

FIG. 5: Effective thickness versus energy curve shown with the two sigma cutoff used to identify alpha particles.

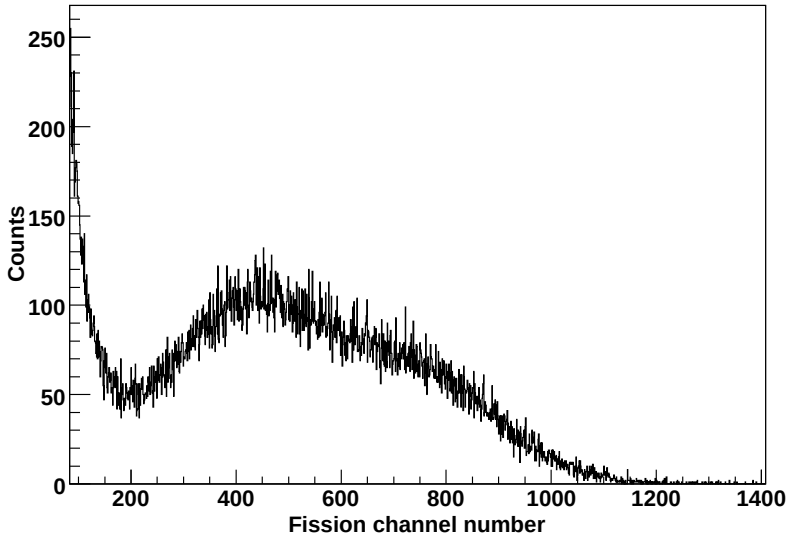

FIG. 6: Typical fission spectrum from a ring in the fission detector.

events to remove light ion contamination. A typical fission spectrum for an individual ring is shown in figure 6. The uncertainty in determining the cut off point at the minimum of the fission spectrum introduces a systematic uncertainty in the final ^{237}U(n,f) cross section. The sensitivity of the final cross section to the fission cutoff point was determined to be 1.3% and is listed in Table I.

For each ring in the ΔE detector a PID plot and range curve were created. The alpha particles, identified in the effective thickness energy plot, in coincidence with fission events were identified by the sort routine. A histogram of alpha-fission coincidences as a function of energy was created for each ring in the ΔE detector. The energy bins for the histogram were chosen to be 100 keV wide. A bin size of 100 keV was chosen due to the statistics per bin and in order to allow for compression at a later time. The alpha particle energy was corrected event by event for energy losses in the target, δ-shield, and inert detector layers (Al and Au). The spectra for each ring were then summed together. This process was identical for both $^{238}U(\alpha,\alpha'f)$ and the $^{236}U(\alpha,\alpha'f)$ data. As mentioned at the end of section II the data were corrected by a factor which takes into account the integrated beam current, number of target atoms, and live time of the acquisition system. This normalization factor is

$$Norm = \frac{I_{^{236}U}}{I_{^{238}U}} \times \frac{T_{Live^{236}U}}{T_{Live^{238}U}} \times \frac{N_{Atoms^{236}U}}{N_{Atoms^{238}U}} = \frac{23410}{50293} \times \frac{0.6304}{0.6017} \times \frac{184}{585} = 0.1534 \qquad (8)$$

TABLE I: Sources of systematic uncertainty for the ^{238}U/^{236}U ratio.

Affected parameter	Source of uncertainty	Relative uncertainty
Normalisation Factor	^{238}U Target thickness	5 %
Normalisation Factor	^{236}U Target thickness	5 %
Alpha spectra	Fission spectrum cutoff energy	1.3 %
Total systematic uncertainty		7.2 %

where $I_{^{23x}U}$ is the integrated beam current, $T_{Live^{23x}U}$ is the live time fraction, and $N_{Atoms^{23x}U}$ are the number of atoms of the corresponding target. The uncertainties associted with the live time fraction and integrated beam current are less than a percent. The uncertainty in the target thicknesses mentioned above is the dominant uncertainty in the normalization factor and is listed in Table I.

The final alpha fission spectra are given by

$$N(E_{ex})_{^{238}Ufission} = N(E_{ex})_{^{238}U\alpha-f} \tag{9}$$

and

$$N(E_{ex})_{^{236}Ufission} = \frac{N(E_{ex})_{^{236}U\alpha-f}}{Norm} \tag{10}$$

where $N(E_{ex})_{^{23x}Ufission}$ are the corrected fission spectra, $N(E_{ex})_{^{23x}U\alpha-f}$ are the alpha fission coincident spectra described above, and $Norm$ is the normalization factor from equation (8). Figure 7 shows the resulting spectra corrected for the normalization factor. The α-U Coulomb barrier (24 MeV) limits the maximum excitation energy that can be studied to 31 MeV (55 MeV - $E_{Coulomb}$).

VI. SYSTEMATIC UNCERTAINTIES

A detailed analysis of the energy loss and uncertainty in the detector system has been performed. The sources of uncertainty are energy straggle, angular resolution, intrinsic detector energy resolution, and cyclotron beam energy resolution and they are documented in Table II. The energy straggle arises from the interaction of the alpha particles with the various materials in the target and detector system. Alpha particles interact with the target material, δ-shield, aluminum and gold layers on the detector, and the silicon. The energy

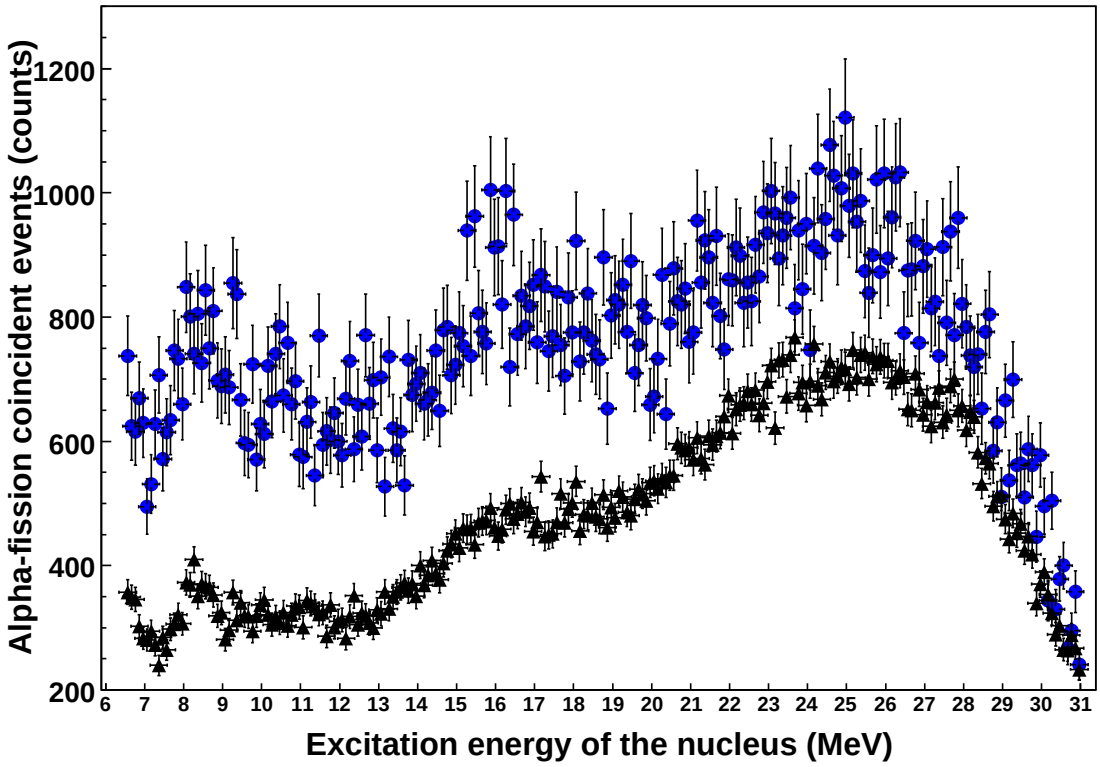

FIG. 7: Number of $(\alpha, \alpha' f)$ events as a function of excitation energy of the respective nucleus. This data is used to calculate relative probability of fission for ^{238}U compared to ^{236}U. The ^{236}U data are represented by circles and the ^{238}U data are shown as triangles.

losses in the inactive layers are substantial (700 keV to 2 MeV) and are corrected for on an event by event basis during the data analysis. The energy loss corrections take into account the energy of the incident alpha particle and the angle at which it is incident. Typical values of energy loss are given in Table III. The angular resolution of the detector is dictated by the geometry of the beam spot on the target and the relative distances of the target to the ΔE and E detectors.

For this experiment, the angular resolution ranged between 0.7^o to 2.2^o. The angular resolution translates into an uncertainty of the recoil angle of the target nucleus. The intrinsic detector resolution was measured using the ^{226}Ra source described in Section IV. The cyclotron beam energy resolution was inferred from the width of the elastic peak in a previous experiment. In that experiment, the beam width was measured by placing a calibrated silicon detector directly in the alpha beam from the 88 Inch Cyclotron [19]. The

TABLE II: Systematic sources of energy uncertainty.

Sources of energy uncertainty	ΔE (keV)
Energy straggle (δ-shield and target)	$38 - 85$
Recoil angle	$19 - 54$
Intrinsic detector energy resolution	$38 - 55$
Cyclotron beam	60
Total uncertainty	157 - 220

TABLE III: Materials responsible for energy loss.

Detector Element	Material	Areal Density ($\frac{\mu g}{cm^2}$)	E_{loss} (keV)
^{238}U Target	^{238}U	292	18 - 52
^{236}U Target	^{238}U	92	6 - 15
^{181}Ta Backing	^{181}Ta	2300	150 - 418
Delta Shield	Aluminum	4440	508 - 1534
Detector Contacts (sectors)	Gold	1158	73 - 200
Detector Contacts (rings)	Aluminum	27	19 - 33
Total energy loss for ^{238}U target and detector			682 - 1744
Total energy loss for ^{236}U target and detector			838 - 2128

energy width of the cyclotron beam was then inferred using the following relation

$$\Delta E^2_{total} = \Delta E^2_{cal} + \Delta E^2_{beam} \tag{11}$$

where E_{total} is the total energy uncertainty, E_{cal} is the intrinsic detector resolution, and E_{beam} is the Cyclotron beam energy width. The energy uncertainty changes as a function of outgoing alpha particle angle, therefore the energy straggle and recoil angle uncertainty partially cancel each other. As a final check on the energy uncertainty, the elastic peak was fit with a gaussian and the one sigma uncertainty was found to be 220 keV. Based on this and the above calculations the overall energy uncertainty used in the final cross section was taken to be 220 keV.

One further concern is the anisotropy of the angular distribution of the fission frag-

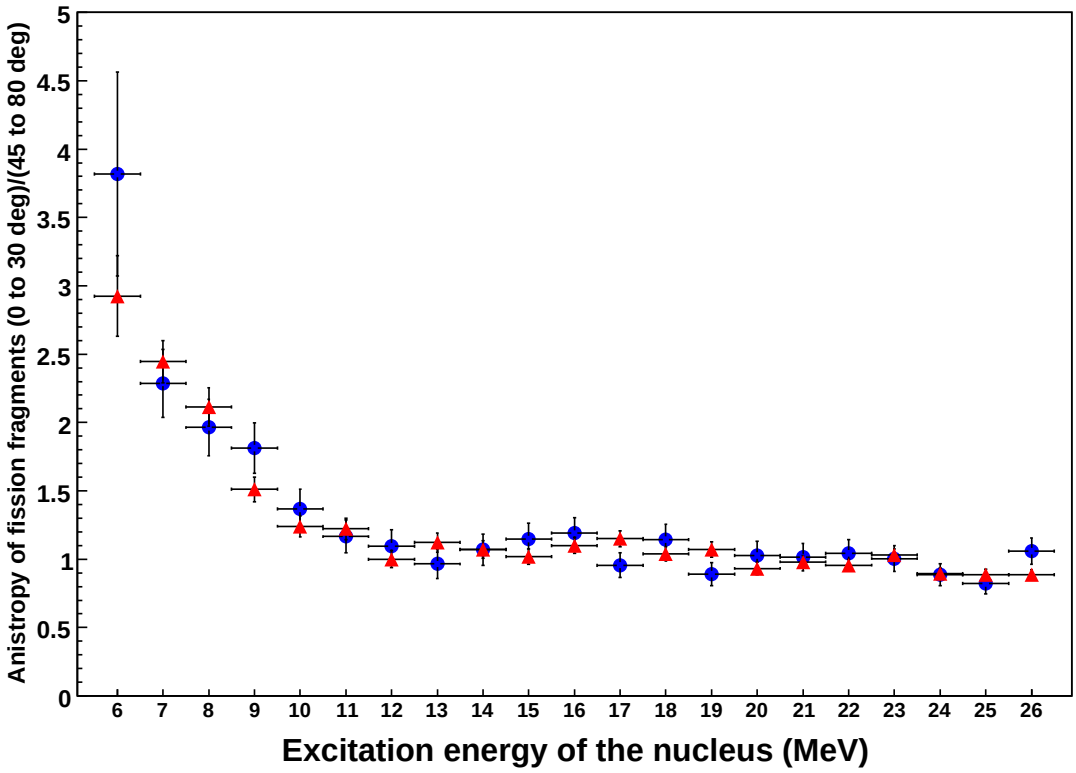

FIG. 8: Plotted are the in-plane fission fragment anisotropies as a function of excitation energy of the nucleus for ^{238}U (red triangles) and ^{236}U (blue circles). The anisotropy is most pronounced at the fission barrier E_{ex} of approximately 6 MeV and decreases to unity thereafter. The fission anisotropies are equal within uncertainty over the excitation energy range of interest.

ments [16]. A difference in the anisotropies of the fission fragments in the two reactions could lead to differing fission fragment detector efficiencies as a function of energy. This would occur due to the finite solid angle coverage of the fission detector. The fission fragment anisotropies for ^{238}U and ^{236}U fission fragments have been examined as shown in figure 8. As a measure of the anisotropy, we consider the ratio of the number of fission events in the angular range of 0^o to 30^o to the number of fission events over the angle range of 45^o to 80^o, as a function of excitation energy of the nucleus as shown in figure 8. In the energy range near the fission barrier, from 0 to 4 MeV surrogate neutron energy (6.4 to 10.4 MeV excitation energy) , the anisotropy peaked at a factor of 3 and dropped to unity by 4 MeV surrogate neutron energy for both nuclei. The main feature to note is that the ratio of the fission fragment anisotropies of ^{238}U over ^{236}U was found to be consistent with

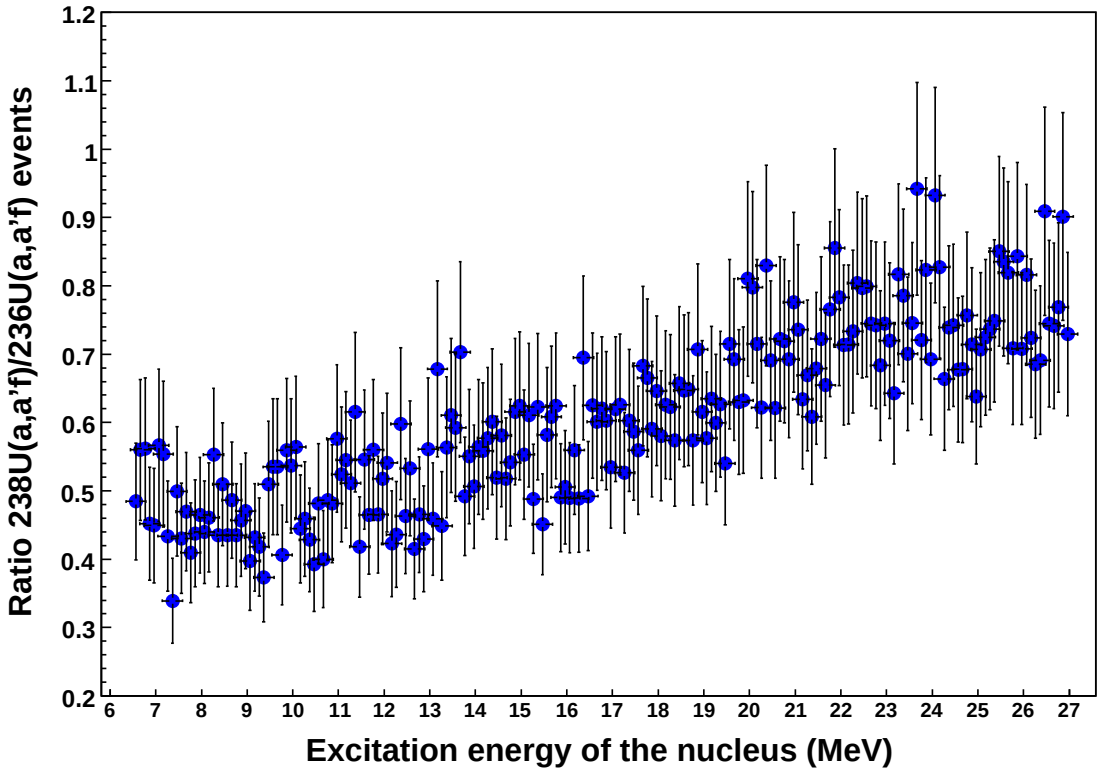

FIG. 9: The plot shows the ratio of $^{238}U(\alpha,\alpha' f)$ to $^{238}U(\alpha,\alpha' f)$ events as a function of excitation energy of the corresponding nucleus.

unity in the energy range from 0 to 20 MeV surrogate neutron energy. The ratio method reduces our sensitivity to the fission fragment anisotropies provided the two nuclei have similar distributions as is the case here.

VII. DETERMINING THE ^{237}U(N,F) CROSS SECTION

The ^{237}U(n,f) cross section was determined from the data using the same procedure as outlined in Section II. The normalized ratio $R(\frac{238}{236}) = N(E_{ex})^{238}U_{fission}/N(E_{ex})^{236}U_{fission}$ was determined as a function of excitation energy as is plotted in figure 9. The ^{235}U(n,f) cross section energy scale was shifted to excitation energy by adding the ^{236}U neutron separation energy (Sn = 6544.5 keV). The product of the $R(\frac{238}{236})$ ratio and the shifted $^{235}U(E_{ex})$ spectrum yields the $^{237}U(E_{ex},n,f)$ spectrum in excitation energy. The final result is obtained by shifting the $^{237}U(E_{ex},n,f)$ energy scale down by subtracting the ^{238}U neutron separation

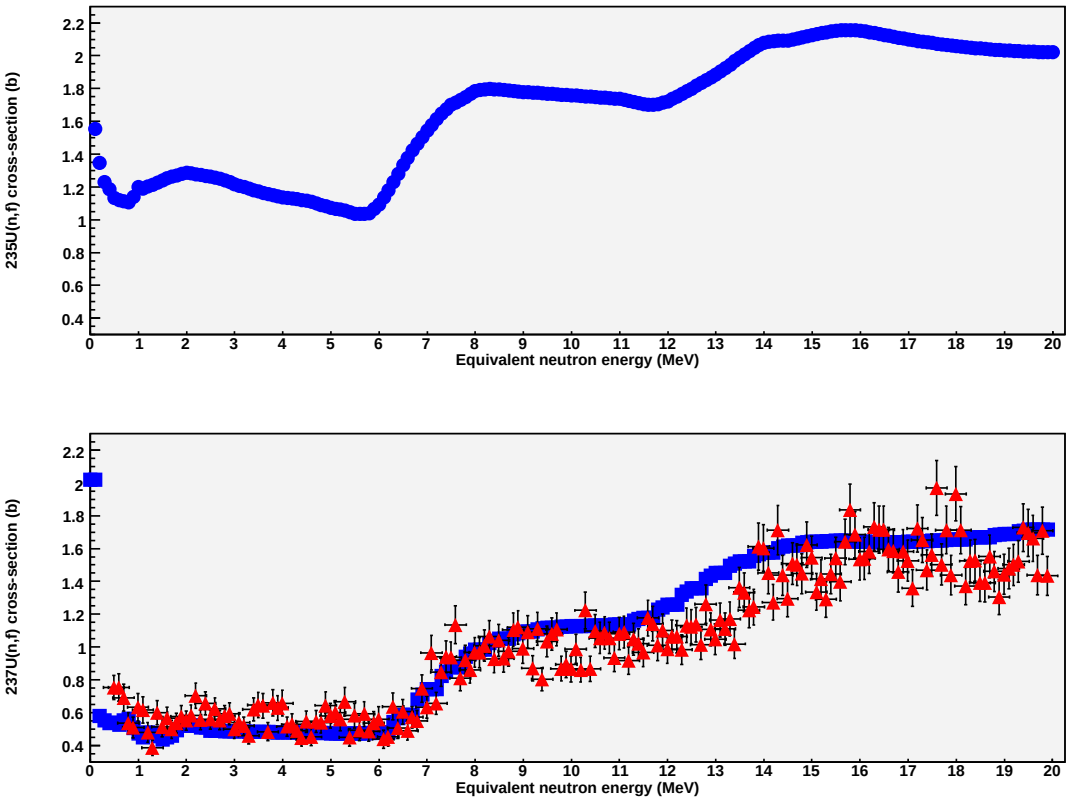

FIG. 10: The upper plot shows the ^{235}U(n,f) cross section from ENDF/B-VII [17] used to determine the ^{237}U(n,f) cross section. The lower plot compares our ^{237}U(n,f) cross section (triangles), to the results from earlier work by Younes and Britt [18] (squares, no error bars shown).

energy ($S_n = 6152.0$ MeV) to obtain the $^{237}U(n,f)$ cross section at the appropriate neutron energy. This procedure is summarized in the following equations.

$$^{235}U(E_{ex}, n, f) = {}^{235}U((E_n + S_n(^{236}U)), n, f) \tag{12}$$

$$^{237}U(E_{ex}, n, f) = \frac{^{238}U(E_{ex}, \alpha, \alpha' f)}{^{236}U(E_{ex}, \alpha, \alpha' f)} \times {}^{235}U(E_{ex}, n, f) \tag{13}$$

$$^{237}U(E_n, n, f) = {}^{237}U((E_{ex} - S_n(^{238}U)), n, f) \tag{14}$$

The upper panel of figure 10 shows the the ^{235}U(n,f) cross section [17] used to obtain the ^{237}U(n,f) cross section. The resulting cross section is plotted in the lower panel of figure 10. For completeness, the previous results from Younes and Britt [18] are also shown. The

two cross sections agree well in the neutron energy range from 0 to approximately 10 MeV. Above 10 MeV our cross section is lower by approximately 10% to 20%. This difference may arise from the linear extrapolation to higher energies of first chance fission used by Younes and Britt.

VIII. CONCLUSIONS

The ^{237}U(n,f) cross section has been determined using the Surrogate Ratio method. This method requires that a fission cross section, for a similar nucleus, be known. In this experiment, the reaction $^{238}U(\alpha, \alpha' f)$ was used as a surrogate reaction for ^{237}U(n,f) and $^{236}U(\alpha, \alpha' f)$ as a surrogate reaction for the known case of ^{235}U(n,f). In using the Surrogate Ratio method, the assumption has been made that the inelastic (α, α') scattering cross section for the two nuclei (^{238}U and ^{236}U) are equal to within approximately 5%. We have also assumed that the compound nucleus formation at equivalent neutron energies in the range from 0 MeV to 20 MeV are equal to within approximately 5%. These two assumptions lead to an uncertainty in the ^{237}U(n,f) cross section no greater than 10% over the energy range from 0 to 20 MeV equivalent neutron energy. The Surrogate Ratio method minimizes pre-equilibrium effects in the final cross section. Furthermore, it reduces our sensitivity to the anisotropy distribution of the fission fragments provided the nuclei have similar recoil angles and initial spin populations.

Acknowledgments

We wish to acknowledge the useful discussions and advice of H.C. Britt, J. Willhemy, and W. Younes. We would like to thank the 88 Inch Cyclotron operations and facilities staff for their help in performing this experiment. We also want to thank F. Howland for his effort and expertise in designing the STARS scattering chamber and R. Foreman for his efforts in manufacturing our self-supporting ^{238}U targets. This work was performed under the auspices of the U.S. Department of Energy by the University of California, Lawrence Livermore National Laboratory under contract No. W-7405-Eng-48 and Lawrence Berkeley National Laboratory under contract No. DE-AC03-76SF0098.

APPENDIX A: U237(N,F) CROSS SECTION

TABLE IV: This table lists the ^{237}U(n,f) cross section derived relative to the ^{235}U(n,f) cross section using the Surrogate Ratio method in 100 keV steps. Column 1 is the equivalent neutron energy of the cross section. The ^{237}U(n,f) cross section is listed in column 3 followed by the experimental statistical uncertainty and the experimental systematic uncertainty in columns 4 and 5 respectively. Note there is currently at most a 10% systematic uncertainty due to the underlying theory [2]. This is not included in the total uncertainty listed in column 6. For comparison, the ^{235}U(n,f) cross section is listed in column 7.

Equivalent Neutron Energy (MeV)	Energy Unc. (MeV)	^{237}U(n,f) (barns)	Statistical Unc. (barns)	Systematic Unc. (barns)	Total Unc. (barns)	^{235}U(n,f) (barns)
0.493	0.220	0.753	0.051	0.054	0.074	1.554
0.593	0.220	0.754	0.063	0.054	0.083	1.347
0.693	0.220	0.691	0.064	0.050	0.081	1.230
0.793	0.220	0.536	0.050	0.038	0.063	1.187
0.893	0.220	0.509	0.051	0.037	0.063	1.133
0.993	0.220	0.634	0.071	0.046	0.084	1.118
1.093	0.220	0.616	0.067	0.044	0.080	1.112
1.193	0.220	0.479	0.050	0.034	0.060	1.105
1.293	0.220	0.386	0.038	0.028	0.047	1.139
1.393	0.220	0.598	0.059	0.043	0.073	1.199
1.493	0.220	0.513	0.050	0.037	0.062	1.191
1.593	0.220	0.565	0.053	0.041	0.067	1.202
1.693	0.220	0.498	0.044	0.036	0.056	1.214
1.793	0.220	0.537	0.047	0.039	0.061	1.226
1.893	0.220	0.576	0.051	0.041	0.066	1.241

TABLE IV: (continued)

Equivalent Neutron Energy (MeV)	Energy Unc. (MeV)	^{237}U(n,f) (barns)	Statistical Unc. (barns)	Systematic Unc. (barns)	Total Unc. (barns)	^{235}U(n,f) (barns)
1.993	0.220	0.551	0.043	0.040	0.059	1.254
2.093	0.220	0.582	0.047	0.042	0.063	1.262
2.193	0.220	0.703	0.057	0.050	0.076	1.270
2.293	0.220	0.556	0.044	0.040	0.060	1.278
2.393	0.220	0.656	0.053	0.047	0.071	1.287
2.493	0.220	0.558	0.043	0.040	0.059	1.282
2.593	0.220	0.622	0.050	0.045	0.067	1.278
2.693	0.220	0.554	0.044	0.040	0.059	1.272
2.793	0.220	0.579	0.049	0.042	0.065	1.266
2.893	0.220	0.594	0.051	0.043	0.067	1.262
2.993	0.220	0.500	0.043	0.036	0.056	1.258
3.093	0.220	0.540	0.047	0.039	0.061	1.249
3.193	0.220	0.519	0.041	0.037	0.056	1.241
3.293	0.220	0.459	0.038	0.033	0.050	1.228
3.393	0.220	0.620	0.055	0.045	0.071	1.216
3.493	0.220	0.646	0.061	0.046	0.077	1.207
3.593	0.220	0.641	0.061	0.046	0.076	1.198
3.693	0.220	0.483	0.044	0.035	0.056	1.190
3.793	0.220	0.660	0.065	0.047	0.081	1.181
3.893	0.220	0.629	0.060	0.045	0.075	1.172
3.993	0.220	0.657	0.063	0.047	0.079	1.164
4.093	0.220	0.514	0.047	0.037	0.060	1.157
4.193	0.220	0.528	0.051	0.038	0.063	1.150
4.293	0.220	0.490	0.045	0.035	0.057	1.143
4.393	0.220	0.446	0.041	0.032	0.052	1.136
4.493	0.220	0.545	0.053	0.039	0.066	1.132

TABLE IV: (continued)

Equivalent Neutron Energy (MeV)	Energy Unc. (MeV)	^{237}U(n,f) (barns)	Statistical Unc. (barns)	Systematic Unc. (barns)	Total Unc. (barns)	^{235}U(n,f) (barns)
4.593	0.220	0.451	0.042	0.032	0.053	1.128
4.693	0.220	0.547	0.053	0.039	0.066	1.125
4.793	0.220	0.539	0.052	0.039	0.064	1.121
4.893	0.220	0.644	0.066	0.046	0.081	1.117
4.993	0.220	0.581	0.061	0.042	0.074	1.109
5.093	0.220	0.600	0.061	0.043	0.074	1.100
5.193	0.220	0.558	0.056	0.040	0.069	1.091
5.293	0.220	0.665	0.073	0.048	0.087	1.082
5.393	0.220	0.448	0.043	0.032	0.054	1.073
5.493	0.220	0.582	0.063	0.042	0.075	1.067
5.593	0.220	0.494	0.053	0.035	0.064	1.062
5.693	0.220	0.592	0.063	0.042	0.076	1.057
5.793	0.220	0.487	0.052	0.035	0.063	1.047
5.893	0.220	0.537	0.059	0.039	0.071	1.037
5.993	0.220	0.561	0.062	0.040	0.074	1.036
6.093	0.220	0.437	0.047	0.031	0.056	1.035
6.193	0.220	0.453	0.046	0.033	0.056	1.038
6.293	0.220	0.637	0.068	0.046	0.082	1.065
6.393	0.220	0.505	0.051	0.036	0.063	1.091
6.493	0.220	0.605	0.060	0.043	0.074	1.135
6.593	0.220	0.489	0.043	0.035	0.056	1.179
6.693	0.220	0.572	0.051	0.041	0.066	1.229
6.793	0.220	0.550	0.047	0.040	0.061	1.281
6.893	0.220	0.748	0.064	0.054	0.083	1.333
6.993	0.220	0.632	0.049	0.045	0.067	1.378
7.093	0.220	0.965	0.080	0.069	0.106	1.423

TABLE IV: (continued)

Equivalent Neutron Energy (MeV)	Energy Unc. (MeV)	^{237}U(n,f) (barns)	Statistical Unc. (barns)	Systematic Unc. (barns)	Total Unc. (barns)	^{235}U(n,f) (barns)
7.193	0.220	0.657	0.047	0.047	0.067	1.464
7.293	0.220	0.847	0.062	0.061	0.087	1.503
7.393	0.220	0.942	0.069	0.068	0.097	1.542
7.493	0.220	0.936	0.066	0.067	0.094	1.579
7.593	0.220	1.135	0.082	0.082	0.116	1.615
7.693	0.220	0.810	0.051	0.058	0.077	1.647
7.793	0.220	0.921	0.059	0.066	0.088	1.674
7.893	0.220	0.861	0.054	0.062	0.082	1.700
7.993	0.220	0.968	0.058	0.070	0.091	1.715
8.093	0.220	0.966	0.060	0.069	0.092	1.730
8.193	0.220	1.009	0.062	0.072	0.095	1.747
8.293	0.220	1.062	0.063	0.076	0.099	1.766
8.393	0.220	0.927	0.053	0.067	0.085	1.785
8.493	0.220	1.041	0.063	0.075	0.097	1.790
8.593	0.220	0.930	0.052	0.067	0.085	1.795
8.693	0.220	0.973	0.054	0.070	0.088	1.797
8.793	0.220	1.105	0.063	0.079	0.101	1.795
8.893	0.220	1.120	0.063	0.080	0.102	1.793
8.993	0.220	0.990	0.055	0.071	0.090	1.790
9.093	0.220	1.092	0.061	0.078	0.099	1.787
9.193	0.220	0.872	0.045	0.063	0.077	1.785
9.293	0.220	1.110	0.062	0.080	0.101	1.782
9.393	0.220	0.803	0.041	0.058	0.071	1.779
9.493	0.220	1.034	0.056	0.074	0.093	1.777
9.593	0.220	1.080	0.060	0.078	0.098	1.775
9.693	0.220	1.107	0.062	0.079	0.101	1.773

TABLE IV: (continued)

Equivalent Neutron Energy (MeV)	Energy Unc. (MeV)	^{237}U(n,f) (barns)	Statistical Unc. (barns)	Systematic Unc. (barns)	Total Unc. (barns)	^{235}U(n,f) (barns)
9.793	0.220	0.868	0.044	0.062	0.076	1.771
9.893	0.220	0.894	0.047	0.064	0.079	1.769
9.993	0.220	0.865	0.045	0.062	0.077	1.767
10.093	0.220	0.988	0.054	0.071	0.089	1.765
10.193	0.220	0.861	0.043	0.062	0.076	1.763
10.293	0.220	1.223	0.070	0.088	0.112	1.761
10.393	0.220	0.866	0.045	0.062	0.077	1.759
10.493	0.220	1.097	0.061	0.079	0.100	1.757
10.593	0.220	1.055	0.057	0.076	0.095	1.754
10.693	0.220	1.087	0.061	0.078	0.099	1.752
10.793	0.220	1.055	0.058	0.076	0.095	1.750
10.893	0.220	0.934	0.051	0.067	0.084	1.748
10.993	0.220	1.081	0.061	0.078	0.099	1.745
11.093	0.220	1.091	0.058	0.078	0.098	1.743
11.193	0.220	0.917	0.050	0.066	0.083	1.741
11.293	0.220	1.048	0.061	0.075	0.097	1.739
11.393	0.220	1.019	0.058	0.073	0.093	1.736
11.493	0.220	0.967	0.054	0.069	0.088	1.730
11.593	0.220	1.177	0.068	0.085	0.108	1.724
11.693	0.220	1.142	0.068	0.082	0.106	1.717
11.793	0.220	1.010	0.057	0.073	0.092	1.710
11.893	0.220	1.101	0.063	0.079	0.101	1.703
11.993	0.220	0.988	0.053	0.071	0.089	1.702
12.093	0.220	1.065	0.064	0.076	0.099	1.702
12.193	0.220	1.062	0.061	0.076	0.098	1.706
12.293	0.220	0.983	0.055	0.071	0.089	1.714

TABLE IV: (continued)

Equivalent Neutron Energy (MeV)	Energy Unc. (MeV)	^{237}U(n,f) (barns)	Statistical Unc. (barns)	Systematic Unc. (barns)	Total Unc. (barns)	^{235}U(n,f) (barns)
12.393	0.220	1.132	0.065	0.081	0.104	1.722
12.493	0.220	1.123	0.065	0.081	0.103	1.736
12.593	0.220	1.136	0.066	0.082	0.105	1.751
12.693	0.220	1.014	0.053	0.073	0.090	1.767
12.793	0.220	1.261	0.075	0.091	0.117	1.783
12.893	0.220	1.108	0.060	0.080	0.100	1.799
12.993	0.220	1.048	0.056	0.075	0.094	1.816
13.093	0.220	1.163	0.061	0.084	0.103	1.834
13.193	0.220	1.110	0.057	0.080	0.098	1.851
13.293	0.220	1.171	0.062	0.084	0.104	1.869
13.393	0.220	1.019	0.051	0.073	0.089	1.886
13.493	0.220	1.362	0.073	0.098	0.122	1.906
13.593	0.220	1.333	0.069	0.096	0.118	1.925
13.693	0.220	1.225	0.061	0.088	0.107	1.946
13.793	0.220	1.244	0.062	0.089	0.109	1.967
13.893	0.220	1.611	0.084	0.116	0.143	1.988
13.993	0.220	1.603	0.083	0.115	0.142	2.008
14.093	0.220	1.451	0.072	0.104	0.126	2.029
14.193	0.220	1.272	0.058	0.091	0.108	2.047
14.293	0.220	1.712	0.087	0.123	0.151	2.063
14.393	0.220	1.437	0.067	0.103	0.123	2.080
14.493	0.220	1.294	0.058	0.093	0.109	2.084
14.593	0.220	1.508	0.068	0.108	0.128	2.088
14.693	0.220	1.502	0.068	0.108	0.128	2.090
14.793	0.220	1.447	0.065	0.104	0.123	2.091
14.893	0.220	1.623	0.076	0.117	0.139	2.091

TABLE IV: (continued)

Equivalent Neutron Energy (MeV)	Energy Unc. (MeV)	^{237}U(n,f) (barns)	Statistical Unc. (barns)	Systematic Unc. (barns)	Total Unc. (barns)	^{235}U(n,f) (barns)
14.993	0.220	1.544	0.071	0.111	0.132	2.098
15.093	0.220	1.335	0.057	0.096	0.111	2.106
15.193	0.220	1.413	0.062	0.101	0.119	2.113
15.293	0.220	1.290	0.055	0.093	0.108	2.119
15.393	0.220	1.444	0.062	0.104	0.121	2.126
15.493	0.220	1.540	0.068	0.111	0.130	2.132
15.593	0.220	1.399	0.059	0.100	0.116	2.137
15.693	0.220	1.640	0.073	0.118	0.139	2.142
15.793	0.220	1.837	0.084	0.132	0.156	2.147
15.893	0.220	1.684	0.072	0.121	0.141	2.152
15.993	0.220	1.537	0.066	0.110	0.129	2.154
16.093	0.220	1.540	0.065	0.111	0.128	2.156
16.193	0.220	1.581	0.066	0.114	0.132	2.156
16.293	0.220	1.733	0.075	0.124	0.146	2.155
16.393	0.220	1.715	0.074	0.123	0.144	2.154
16.493	0.220	1.716	0.075	0.123	0.144	2.148
16.593	0.220	1.596	0.067	0.115	0.133	2.143
16.693	0.220	1.586	0.069	0.114	0.133	2.137
16.793	0.220	1.457	0.060	0.105	0.121	2.132
16.893	0.220	1.583	0.066	0.114	0.132	2.126
16.993	0.220	1.526	0.062	0.110	0.126	2.121
17.093	0.220	1.360	0.057	0.098	0.113	2.115
17.193	0.220	1.723	0.074	0.124	0.144	2.109
17.293	0.220	1.653	0.070	0.119	0.138	2.104
17.393	0.220	1.470	0.062	0.106	0.122	2.098
17.493	0.220	1.561	0.065	0.112	0.129	2.094

TABLE IV: (continued)

Equivalent Neutron Energy (MeV)	Energy Unc. (MeV)	^{237}U(n,f) (barns)	Statistical Unc. (barns)	Systematic Unc. (barns)	Total Unc. (barns)	^{235}U(n,f) (barns)
17.593	0.220	1.969	0.088	0.141	0.167	2.090
17.693	0.220	1.503	0.064	0.108	0.126	2.085
17.793	0.220	1.713	0.076	0.123	0.145	2.081
17.893	0.220	1.439	0.062	0.103	0.120	2.077
17.993	0.220	1.934	0.090	0.139	0.166	2.073
18.093	0.220	1.713	0.074	0.123	0.144	2.070
18.193	0.220	1.372	0.057	0.098	0.114	2.066
18.293	0.220	1.524	0.067	0.109	0.128	2.062
18.393	0.220	1.528	0.065	0.110	0.128	2.059
18.493	0.220	1.391	0.057	0.100	0.115	2.055
18.593	0.220	1.391	0.058	0.100	0.116	2.052
18.693	0.220	1.551	0.067	0.111	0.130	2.049
18.793	0.220	1.461	0.062	0.105	0.122	2.046
18.893	0.220	1.304	0.053	0.094	0.107	2.043
18.993	0.220	1.443	0.062	0.104	0.121	2.041
19.093	0.220	1.478	0.062	0.106	0.123	2.039
19.193	0.220	1.501	0.065	0.108	0.126	2.036
19.293	0.220	1.523	0.065	0.109	0.127	2.034
19.393	0.220	1.727	0.078	0.124	0.146	2.032
19.493	0.220	1.695	0.077	0.122	0.144	2.030
19.593	0.220	1.662	0.074	0.119	0.141	2.029
19.693	0.220	1.437	0.061	0.103	0.120	2.027
19.793	0.220	1.709	0.077	0.123	0.145	2.026
19.893	0.220	1.433	0.060	0.103	0.119	2.024
19.993	0.220	1.651	0.074	0.119	0.140	2.024
20.093	0.220	1.464	0.064	0.105	0.123	2.023

APPENDIX B: $^{238}U(\alpha,\alpha'f)$ AND $^{236}U(\alpha,\alpha'f)$ DATA USED TO DERIVE THE ^{237}U(N,F) CROSS SECTION.

TABLE V: Background subtracted and normalized data used to derive the ^{237}U(n,f) cross section in 100 keV steps. The first column denotes the excitation energy of the respective nucleus. The ^{235}U(n,f) cross section [17] is in column 2 and has been shifted to excitation energy. The background subtracted and normalized $^{236}U(\alpha,\alpha'f)$ data are shown in column 3 with its statistical uncertainty in column 4. Column 5 shows the relative uncertainty of each bin (ie: 100 counts in a bin yields a 10% relative uncertainty). Columns 6, 7, and 8 contain the same information for the $^{238}U(\alpha,\alpha'f)$ data.

Excitation Energy (MeV)	^{235}U(n,f) (barns)	$^{236}U(\alpha,\alpha'f)$ (counts)	Stat. Unc. (counts)	Rel. Unc. (%)	$^{238}U(\alpha,\alpha'f)$ (counts)	Stat. Unc. (counts)	Rel. Unc. (%)
6.6	1.6	737.6	63.9	8.7	357.3	19.7	5.5
6.7	1.3	624.2	54.9	8.8	349.6	19.5	5.6
6.8	1.2	615.6	54.2	8.8	345.8	19.3	5.6
6.9	1.2	669.5	58.5	8.7	302.4	18.1	6.0
7.0	1.1	629.5	55.3	8.8	282.8	17.6	6.2
7.1	1.1	495.0	44.5	9.0	280.6	17.5	6.3
7.2	1.1	531.4	47.5	8.9	294.3	17.9	6.1
7.3	1.1	627.5	55.2	8.8	272.2	17.3	6.4
7.4	1.1	706.6	61.4	8.7	239.6	16.4	6.9
7.5	1.2	571.3	50.7	8.9	285.1	17.7	6.2
7.6	1.2	614.7	54.2	8.8	264.5	17.1	6.5
7.7	1.2	634.2	55.7	8.8	297.9	18.1	6.1
7.8	1.2	746.1	64.5	8.6	305.7	18.3	6.0
7.9	1.2	732.9	63.4	8.7	320.8	18.8	5.9
8.0	1.2	659.9	57.8	8.8	306.5	18.4	6.0

TABLE V: (continued)

Excitation Energy (MeV)	^{235}U(n,f) (barns)	$^{236}U(\alpha,\alpha'f)$ (counts)	Stat. Unc. (counts)	Rel. Unc. (%)	$^{238}U(\alpha,\alpha'f)$ (counts)	Stat. Unc. (counts)	Rel. Unc. (%)
8.1	1.3	848.2	72.6	8.6	372.8	20.1	5.4
8.2	1.3	800.6	68.8	8.6	369.2	20.0	5.4
8.3	1.3	740.8	64.1	8.7	409.7	21.0	5.1
8.4	1.3	805.3	69.2	8.6	350.5	19.6	5.6
8.5	1.3	726.3	63.0	8.7	370.2	20.1	5.4
8.6	1.3	843.2	72.2	8.6	366.9	20.0	5.4
8.7	1.3	749.7	64.9	8.7	364.8	20.0	5.5
8.8	1.3	810.1	69.6	8.6	352.7	19.6	5.6
8.9	1.3	698.1	60.8	8.7	319.0	18.8	5.9
9.0	1.3	688.6	60.0	8.7	324.2	18.9	5.8
9.1	1.3	707.1	61.5	8.7	280.9	17.8	6.3
9.2	1.2	686.6	59.8	8.7	296.7	18.2	6.2
9.3	1.2	854.5	73.1	8.6	357.1	19.8	5.6
9.4	1.2	837.0	71.7	8.6	312.5	18.7	6.0
9.5	1.2	666.8	58.3	8.7	340.0	19.4	5.7
9.6	1.2	597.5	52.8	8.8	319.6	18.9	5.9
9.7	1.2	594.3	52.6	8.8	318.1	18.9	5.9
9.8	1.2	724.1	62.8	8.7	294.2	18.2	6.2
9.9	1.2	570.9	50.6	8.9	319.3	19.0	5.9
10.0	1.2	627.9	55.2	8.8	336.9	19.4	5.8
10.1	1.2	611.7	53.9	8.8	345.1	19.6	5.7
10.2	1.2	721.8	62.6	8.7	320.8	19.0	5.9
10.3	1.2	664.1	58.0	8.7	304.8	18.5	6.1
10.4	1.1	740.8	64.1	8.7	317.3	18.9	5.9
10.5	1.1	784.8	67.6	8.6	308.1	18.7	6.1
10.6	1.1	673.8	58.8	8.7	324.5	19.1	5.9

TABLE V: (continued)

Excitation Energy (MeV)	^{235}U(n,f) (barns)	$^{236}U(\alpha,\alpha'f)$ (counts)	Stat. Unc. (counts)	Rel. Unc. (%)	$^{238}U(\alpha,\alpha'f)$ (counts)	Stat. Unc. (counts)	Rel. Unc. (%)
10.7	1.1	758.6	65.5	8.6	303.4	18.5	6.1
10.8	1.1	659.9	57.8	8.8	320.9	19.0	5.9
10.9	1.1	696.9	60.7	8.7	335.4	19.5	5.8
11.0	1.1	578.6	51.2	8.9	333.6	19.4	5.8
11.1	1.1	574.6	51.0	8.9	301.0	18.5	6.2
11.2	1.1	631.1	55.4	8.8	344.1	19.6	5.7
11.3	1.1	663.5	58.0	8.7	339.2	19.5	5.8
11.4	1.1	545.2	48.6	8.9	335.4	19.4	5.8
11.5	1.1	770.2	66.4	8.6	321.9	19.0	5.9
11.6	1.1	594.0	52.5	8.8	324.2	19.2	5.9
11.7	1.1	616.1	54.2	8.8	286.4	18.2	6.4
11.8	1.1	602.0	53.2	8.8	337.0	19.5	5.8
11.9	1.0	645.5	56.6	8.8	300.3	18.5	6.2
12.0	1.0	600.1	52.9	8.8	310.7	18.8	6.1
12.1	1.0	577.9	51.2	8.9	312.8	18.9	6.0
12.2	1.0	668.8	58.5	8.7	282.7	18.1	6.4
12.3	1.0	729.2	63.3	8.7	318.0	19.0	6.0
12.4	1.1	587.6	52.0	8.8	351.5	19.8	5.6
12.5	1.1	658.6	57.6	8.8	305.0	18.7	6.1
12.6	1.1	607.6	53.6	8.8	323.7	19.2	5.9
12.7	1.2	770.6	66.5	8.6	319.7	19.1	6.0
12.8	1.2	660.7	57.8	8.8	307.4	18.8	6.1
12.9	1.3	698.5	60.8	8.7	300.1	18.5	6.2
13.0	1.3	585.8	51.9	8.9	328.7	19.4	5.9
13.1	1.4	703.1	61.2	8.7	322.6	19.2	5.9
13.2	1.4	527.1	47.2	9.0	357.6	20.1	5.6

TABLE V: (continued)

Excitation Energy (MeV)	^{235}U(n,f) (barns)	$^{236}U(\alpha,\alpha' f)$ (counts)	Stat. Unc. (counts)	Rel. Unc. (%)	$^{238}U(\alpha,\alpha' f)$ (counts)	Stat. Unc. (counts)	Rel. Unc. (%)
13.3	1.5	736.1	63.8	8.7	330.3	19.4	5.9
13.4	1.5	620.5	54.7	8.8	349.8	19.9	5.7
13.5	1.5	585.8	51.9	8.9	357.6	20.1	5.6
13.6	1.6	615.6	54.3	8.8	364.8	20.3	5.6
13.7	1.6	529.3	47.4	9.0	372.0	20.4	5.5
13.8	1.6	731.4	63.5	8.7	359.9	20.2	5.6
13.9	1.7	674.4	59.0	8.7	371.1	20.4	5.5
14.0	1.7	692.6	60.4	8.7	350.7	20.0	5.7
14.1	1.7	710.1	61.9	8.7	400.8	21.2	5.3
14.2	1.7	660.4	57.9	8.8	368.7	20.5	5.6
14.3	1.7	666.4	58.3	8.7	384.7	20.9	5.4
14.4	1.8	678.4	59.3	8.7	407.9	21.5	5.3
14.5	1.8	746.3	64.7	8.7	387.4	21.0	5.4
14.6	1.8	649.1	57.0	8.8	377.3	20.8	5.5
14.7	1.8	779.1	67.3	8.6	403.6	21.4	5.3
14.8	1.8	783.7	67.6	8.6	424.3	21.9	5.2
14.9	1.8	706.1	61.6	8.7	434.9	22.2	5.1
15.0	1.8	723.0	62.9	8.7	451.4	22.5	5.0
15.1	1.8	774.0	66.9	8.6	428.2	22.0	5.1
15.2	1.8	753.5	65.2	8.7	460.3	22.8	4.9
15.3	1.8	939.1	79.8	8.5	458.6	22.7	5.0
15.4	1.8	737.8	64.1	8.7	459.6	22.8	5.0
15.5	1.8	962.1	81.6	8.5	434.3	22.2	5.1
15.6	1.8	805.9	69.4	8.6	469.1	23.0	4.9
15.7	1.8	776.2	67.0	8.6	472.1	23.0	4.9
15.8	1.8	757.3	65.6	8.7	472.9	23.1	4.9

TABLE V: (continued)

Excitation Energy (MeV)	^{235}U(n,f) (barns)	$^{236}U(\alpha,\alpha'f)$ (counts)	Stat. Unc. (counts)	Rel. Unc. (%)	$^{238}U(\alpha,\alpha'f)$ (counts)	Stat. Unc. (counts)	Rel. Unc. (%)
15.9	1.8	1004.9	84.9	8.5	492.6	23.5	4.8
16.0	1.8	911.8	77.7	8.5	460.9	22.8	5.0
16.1	1.8	914.2	77.9	8.5	447.7	22.6	5.0
16.2	1.8	820.0	70.5	8.6	459.0	22.8	5.0
16.3	1.8	1003.1	84.8	8.5	490.1	23.5	4.8
16.4	1.8	719.7	62.6	8.7	499.9	23.6	4.7
16.5	1.8	964.6	81.8	8.5	475.0	23.2	4.9
16.6	1.8	772.9	66.9	8.7	482.9	23.3	4.8
16.7	1.8	834.4	71.7	8.6	501.6	23.8	4.7
16.8	1.8	784.9	67.7	8.6	486.8	23.5	4.8
16.9	1.8	818.0	70.4	8.6	492.9	23.5	4.8
17.0	1.7	851.8	73.0	8.6	455.3	22.7	5.0
17.1	1.7	759.3	65.8	8.7	470.4	23.1	4.9
17.2	1.7	867.5	74.3	8.6	543.1	24.6	4.5
17.3	1.7	849.0	72.8	8.6	447.1	22.6	5.1
17.4	1.7	745.3	64.6	8.7	449.4	22.6	5.0
17.5	1.7	769.2	66.5	8.7	451.3	22.6	5.0
17.6	1.7	840.4	72.0	8.6	470.0	23.0	4.9
17.7	1.7	755.0	65.4	8.7	515.5	24.0	4.7
17.8	1.7	705.2	61.5	8.7	469.1	23.0	4.9
17.9	1.7	831.9	71.4	8.6	491.3	23.5	4.8
18.0	1.7	775.6	67.0	8.6	501.2	23.6	4.7
18.1	1.7	922.4	78.4	8.5	535.5	24.4	4.6
18.2	1.7	728.6	63.3	8.7	456.1	22.6	5.0
18.3	1.7	775.0	66.9	8.6	482.7	23.2	4.8
18.4	1.7	838.2	71.9	8.6	480.9	23.2	4.8

TABLE V: (continued)

Excitation Energy (MeV)	^{235}U(n,f) (barns)	$^{236}U(\alpha,\alpha' f)$ (counts)	Stat. Unc. (counts)	Rel. Unc. (%)	$^{238}U(\alpha,\alpha' f)$ (counts)	Stat. Unc. (counts)	Rel. Unc. (%)
18.5	1.7	762.1	66.0	8.7	501.1	23.6	4.7
18.6	1.7	740.0	64.2	8.7	478.4	23.1	4.8
18.7	1.8	732.2	63.5	8.7	475.0	23.1	4.9
18.8	1.8	896.1	76.4	8.5	514.1	23.9	4.7
18.9	1.8	652.9	57.3	8.8	461.6	22.8	4.9
19.0	1.8	802.7	69.1	8.6	494.3	23.5	4.8
19.1	1.8	827.4	71.0	8.6	477.2	23.1	4.8
19.2	1.8	819.8	70.4	8.6	520.2	24.0	4.6
19.3	1.9	852.3	72.9	8.6	511.1	23.7	4.6
19.4	1.9	775.8	67.0	8.6	486.1	23.3	4.8
19.5	1.9	890.4	76.0	8.5	480.8	23.0	4.8
19.6	1.9	709.7	61.7	8.7	507.2	23.7	4.7
19.7	1.9	755.0	65.4	8.7	522.7	24.0	4.6
19.8	1.9	819.1	70.3	8.6	515.9	23.9	4.6
19.9	2.0	798.1	68.7	8.6	504.8	23.6	4.7
20.0	2.0	659.0	57.8	8.8	534.0	24.2	4.5
20.1	2.0	672.3	58.8	8.7	536.4	24.3	4.5
20.2	2.0	732.6	63.6	8.7	523.8	24.0	4.6
20.3	2.0	868.3	74.2	8.5	539.7	24.3	4.5
20.4	2.1	643.8	56.6	8.8	534.1	24.2	4.5
20.5	2.1	789.6	68.1	8.6	545.5	24.5	4.5
20.6	2.1	878.1	75.0	8.5	545.3	24.4	4.5
20.7	2.1	825.2	70.9	8.6	596.1	25.4	4.3
20.8	2.1	820.4	70.5	8.6	589.6	25.4	4.3
20.9	2.1	845.9	72.5	8.6	585.6	25.3	4.3
21.0	2.1	760.0	65.8	8.7	589.8	25.4	4.3

TABLE V: (continued)

Excitation Energy (MeV)	^{235}U(n,f) (barns)	$^{236}U(\alpha,\alpha' f)$ (counts)	Stat. Unc. (counts)	Rel. Unc. (%)	$^{238}U(\alpha,\alpha' f)$ (counts)	Stat. Unc. (counts)	Rel. Unc. (%)
21.1	2.1	775.2	67.0	8.6	570.2	25.0	4.4
21.2	2.1	955.6	81.1	8.5	606.0	25.6	4.2
21.3	2.1	855.5	73.3	8.6	572.3	25.0	4.4
21.4	2.1	923.8	78.6	8.5	562.3	24.7	4.4
21.5	2.1	896.1	76.4	8.5	608.6	25.7	4.2
21.6	2.1	823.2	70.7	8.6	594.8	25.4	4.3
21.7	2.1	930.3	79.1	8.5	608.8	25.8	4.2
21.8	2.1	801.6	69.1	8.6	613.8	25.7	4.2
21.9	2.1	748.1	64.8	8.7	640.0	26.3	4.1
22.0	2.2	860.6	73.6	8.6	673.6	26.9	4.0
22.1	2.2	859.1	73.6	8.6	612.9	25.8	4.2
22.2	2.2	912.2	77.6	8.5	651.5	26.5	4.1
22.3	2.2	899.0	76.7	8.5	659.1	26.6	4.0
22.4	2.2	822.8	70.7	8.6	661.5	26.7	4.0
22.5	2.2	855.2	73.2	8.6	681.2	27.0	4.0
22.6	2.1	825.2	70.9	8.6	659.4	26.6	4.0
22.7	2.1	916.4	78.0	8.5	682.7	27.1	4.0
22.8	2.1	865.3	74.0	8.5	642.1	26.3	4.1
22.9	2.1	968.6	82.1	8.5	661.8	26.8	4.0
23.0	2.1	935.2	79.5	8.5	696.2	27.4	3.9
23.1	2.1	1003.2	84.8	8.4	722.0	27.8	3.9
23.2	2.1	966.9	81.9	8.5	621.5	26.0	4.2
23.3	2.1	894.3	76.3	8.5	730.5	28.0	3.8
23.4	2.1	931.1	79.1	8.5	731.5	28.0	3.8
23.5	2.1	959.5	81.4	8.5	672.1	26.9	4.0
23.6	2.1	992.1	83.9	8.5	739.4	28.2	3.8

TABLE V: (continued)

Excitation Energy (MeV)	^{235}U(n,f) (barns)	$^{236}U(\alpha,\alpha' f)$ (counts)	Stat. Unc. (counts)	Rel. Unc. (%)	$^{238}U(\alpha,\alpha' f)$ (counts)	Stat. Unc. (counts)	Rel. Unc. (%)
23.7	2.1	814.5	70.0	8.6	767.3	28.6	3.7
23.8	2.1	939.6	79.8	8.5	677.2	27.0	4.0
23.9	2.1	844.9	72.5	8.6	695.4	27.3	3.9
24.0	2.1	950.2	80.6	8.5	658.3	26.7	4.1
24.1	2.1	747.1	64.8	8.7	696.8	27.4	3.9
24.2	2.1	914.7	77.8	8.5	756.9	28.5	3.8
24.3	2.1	1039.1	87.6	8.4	689.9	27.2	3.9
24.4	2.1	903.4	77.0	8.5	667.5	26.7	4.0
24.5	2.1	957.7	81.3	8.5	711.1	27.5	3.9
24.6	2.1	1076.7	90.4	8.4	728.8	27.9	3.8
24.7	2.1	1027.9	86.7	8.4	696.9	27.3	3.9
24.8	2.0	931.5	79.2	8.5	705.1	27.5	3.9
24.9	2.0	1007.2	85.0	8.4	718.9	27.7	3.9
25.0	2.0	1121.5	94.0	8.4	715.7	27.7	3.9
25.1	2.0	979.1	82.9	8.5	692.1	27.2	3.9
25.2	2.0	1030.9	86.9	8.4	747.3	28.3	3.8
25.3	2.0	953.4	80.9	8.5	702.6	27.5	3.9
25.4	2.0	987.2	83.5	8.5	739.0	28.2	3.8
25.5	2.0	873.8	74.6	8.5	742.9	28.2	3.8
25.6	2.0	839.2	72.0	8.6	700.6	27.4	3.9
25.7	2.0	899.4	76.6	8.5	736.7	28.0	3.8
25.8	2.0	1021.5	86.2	8.4	724.1	27.8	3.8
25.9	2.0	872.5	74.6	8.6	736.0	28.0	3.8
26.0	2.0	1031.2	87.0	8.4	730.1	27.9	3.8
26.1	2.0	894.3	76.3	8.5	729.6	27.9	3.8
26.2	2.0	960.3	81.4	8.5	694.9	27.3	3.9

TABLE V: (continued)

Excitation Energy (MeV)	^{235}U(n,f) (barns)	$^{236}U(\alpha,\alpha' f)$ (counts)	Stat. Unc. (counts)	Rel. Unc. (%)	$^{238}U(\alpha,\alpha' f)$ (counts)	Stat. Unc. (counts)	Rel. Unc. (%)
26.3	2.0	1024.5	86.4	8.4	702.0	27.4	3.9
26.4	2.0	1032.6	87.1	8.4	713.6	27.6	3.9
26.5	2.0	774.0	66.9	8.6	703.5	27.5	3.9
26.6	2.0	875.2	74.8	8.5	651.5	26.5	4.1

[1] C. Plettner *et al.*, Phys. Rev. C in press (2005).

[2] J. Escher and F. S. Dietrich, "Examination of the Validity of the Surrogate Ratio Method for Determining (n,f) and (n,γ) Cross Sections of Actinides," LLNL Technical Report, UCRL-TR-212509-Draft (2005) (unpublished).

[3] J. Escher and F. S. Dietrich, "Determining Cross Sections for Reactions on Unstable Nuclei: A Consideration of Indirect Approaches," Second Argonne/MSU/JINA/INT RIA Workshop: Reaction Mechanisms for Rare Isotope Beams (Michigan State University, East Lansing, March 9–12, 2005), AIP Conference Proceedings, submitted (2005), UCRL-PROC-212586.

[4] J. Escher *et al.*, Nucl. Phys. A **758** (2005) 86c–89c.

[5] J. Escher *et al.*, "Surrogate Nuclear Reactions - an Indirect Method for Determining Reaction Cross Sections,"accepted for publication in Jour. Phys. G (2005), UCRL-JRNL-210888.

[6] C. Forssén *et al.*, Nucl. Phys. A **758** (2005) 130c-133c.

[7] J. A. Church et al., Nucl. Phys. A **758** (2005) 126c–129c.

[8] W. Younes and H. C. Britt, Phys. Rev. C **67**, 024610 (2003).

[9] W. Younes and H. C. Britt, Phys. Rev. C **68**, 034610 (2003).

[10] W. Younes, H. C. Britt, J. A. Becker, and J. B. Wilhelmy, Technical Report No. UCRL-ID-154194, Lawrence Livermore National Laboratory, Livermore, CA, 2003 (unpublished).

[11] J. D. Cramer and H. C. Britt, Phys. Rev. C **2**, 2350 (1970).

[12] J. D. Cramer and H. C. Britt, Nucl. Sci. and Eng. **41**, 177 (1970).

[13] H. C. Britt and J. B. Wilhelmy, Nucl. Sci. and Eng. **72**, 222 (1979).

[14] F. S. Dietrich, Technical Report No. UCRL-TR-201718, Lawrence Livermore National Laboratory, Livermore, CA, 2004 (unpublished).

[15] E. Gadioli and P. E. Hodgson, *Pre-Equilibrium Nuclear Reactions* (Clarendon Press, Oxford, 1992).

[16] R. Vandenbosch and J.R. Huizenga, *Nuclear Fission* (Academic Press, New York, 1973).

[17] Young, Chadwick, Talou, and Leal, ENDF/BVII β0 evaluation, MAT # 9228, Mar 2005.

[18] W. Younes and H.C. Britt, Tech. Rep. UCRL-TR-212600, Lawrence Livermore National Laboratory, (2005).

[19] J.T. Burke and L.W. Phair, private communication, (2005).